ELSEVIER

Tectonophysics 281 (1997) 141–161

TECTONOPHYSICS

Microstructure effects on microcracking and brittle failure of dolomites

Yossef. H. Hatzor [a,*], Alon Zur [a], Yaakov Mimran [b]

[a] *Department of Geological and Environmental Sciences, The Deichmann Rock Mechanics Laboratory of the Negev, Ben-Gurion University of the Negev, Beer-Sheva 84105, Israel*

[b] *Geological Survey of Israel, Jerusalem, Israel*

Received 5 August 1996; accepted 9 April 1997

Abstract

In this paper the influence of microstructure on crack initiation stress and ultimate strength is investigated using results and analysis of 32 triaxial compression tests performed on cylindrical cores of dolomite samples which exhibit a wide range of grain sizes and mosaic textures. All tests were performed at a constant strain rate, under confining pressures between 0 to 40 MPa. The predictive capability of conventional criteria for ultimate strength which are based on empirical fitting parameters such as cohesion and internal friction angle, or mechanical properties such as unconfined compressive strength, is shown to be quite poor, due to the influence of microstructure. Microstructure controls ultimate strength to such a degree that an assumed mechanical property such as unconfined compressive strength may vary by more than a factor of two, where two different microstructure patterns are present.

The validity of published analytical expressions which predict fracture initiation stress assuming the sliding crack model is tested using both mean and maximum grain size, and inserting the measured fracture initiation stress as the remote stress. It is shown that these approximate models fail to describe true behaviour because they ignore boundary conditions which exist at the tip of the leading crack at different mosaic textures.

Early attempts to discuss the influence of microstructure on rock strength have shown that ultimate strength is inversely related to mean grain size. This study demonstrates that grain size alone can not be used in correlation with ultimate strength. Rather, the combination of both grain size and porosity dominate the mechanical response of the rock. Fracture initiation stress is found to be more sensitive to the influence of grain size than ultimate strength, possibly because the length of initial cracks controls the level of stress concentration at the tip of leading cracks. However, fracture initiation stress is shown to be inversely related to both porosity and mean grain size, thus the importance of porosity in the initiation process must be recognized. Ultimate strength is influenced primarily by porosity and mosaic texture, and is less sensitive to mean grain size, possibly because once fracture propagation is initiated, grain arrangement controls fracture interaction processes which lead to macroscopic failure.

Keywords: micromechanics; brittle failure; dolomites; porosity; grain size

* Corresponding author. Tel.: +972 (7) 647-2621; fax: +972 (2) 647-2997; e-mail: hatzor@bgumail.bgu.ac.il

PII S0040-1951(97)00073-5

1. Introduction

Early workers in rock mechanics have studied the mechanical behaviour of sedimentary rocks under confining pressure, either to determine their ultimate strength (e.g. Handin and Hager, 1957) or to characterize the dominant deformation mechanism (e.g. Handin and Fairbairn, 1955; Weiss and Turner, 1972). Much effort has been dedicated to the prediction of ultimate strength either for engineering applications or for tectonophysical model development.

Ultimate strength prediction was pioneered by Griffith (1921) who has developed a theoretical model for instantaneous fracture of brittle solids under tension, and a modified criterion for failure under compression (Griffith, 1924). Griffith's criterion suffers from several fundamental flaws, one of which is the assumption that crack initiation and ultimate strength are achieved at the same stress level. It is now a well documented experimental fact that crack initiation precedes dilation and unstable crack propagation, each of which are attained at about 40% and 80% of the ultimate stress, respectively (see for example Martin and Chandler, 1994 who tested granitic rocks). Empirical failure criteria were first discussed by Coulomb (1776), the mathematical expression of which is given by the well known Coulomb–Mohr relationship. This criterion postulates that shear strength is comprised of two components, an inherent 'cohesion' which is independent of normal stress, and a frictional component. Both the cohesion and the 'internal friction' angle are purely empirical parameters, the physical nature of which is still somewhat vague. In the engineering literature two well known empirical criteria for the failure of rock under compression were proposed by Bieniawski (1974) and Hoek and Brown (1980). Both criteria incorporate fitting parameters which are lithology-dependent. These more recent criteria are used extensively in engineering analysis and design, but they suffer from a lack of theoretical basis. Furthermore, these criteria are scaled by the unconfined compressive strength of the rock type, which is considered a material property. This, however, is unique to each rock type, and in a single limestone or sandstone formation the value of the unconfined compressive strength may vary according to local textural variations.

A few workers have investigated the influence of the variability in grain size and texture on the mechanical response. Olsson (1974) studied the yield stress of marble and showed that it increases linearly with the inverse square root of the mean grain size. His results are consistent with the Petch (1953) dislocation pileup model. Petch's relationship has been successfully validated for metals. In rocks, however, the predicted linear relationship is seldom found. Hugman and Friedman (1979) found that weighted mean grain size (in carbonates) and micrite content (in limestones) have the highest linear correlation coefficients with ultimate strength. The more comprehensive data analysis of Olsson (1974) suggest that the relationship established by Hugman and Friedman (1979) should be a negative exponential, as can be seen also in the uniaxial test results of Wong et al. (1995); only the correlation with the inverse square root of the mean grain size yields a linear fit, as has been found by Fredrich et al. (1990). The studies mentioned above have used the mean weighted grain size in the interpretation and analysis of data. The physical meaning of the latter term, however, is dubious because in carbonate rocks in general, and particularly in dolomites, the mean grain size is a single value in a relatively broad grain size distribution of the rock matrix.

Analytical expressions for fracture initiation stress were developed by Horii and Nemat-Nasser (1985) and by Ashby and Hallam (1986). These approximate models assume an infinite plate containing a single flaw which slides when a critical shear stress level is attained. These models are attractive because they incorporate a physical flaw in the specimen, which can be a function of grain size, or grain boundary length, thus creating a link with petrography. The weakness of the analytical expressions is the assumption of a continuous plate containing a single flaw only rather than a multitude of grains, and the neglect of intergranular arrangement.

In this paper the influence of grain size, porosity, and mosaic texture on the stresses at which crack initiation ensues and ultimate strength is attained are investigated using 32 cylindrical cores of dolomites which were tested under confining pressures between 0 and 40 MPa. The predictive capability of available failure (ultimate strength) criteria are tested and the discrepancies with observations are discussed. The

grain size effect is reviewed here with respect to dolomites of diverse grain size distributions. It is concluded that grain size alone yields poor correlation with ultimate strength, and a slightly better correlation with crack initiation stress. The predictions of available fracture mechanics models are tested, and the relationship between the required critical flaw length ($2a$) for fracture initiation under a given remote stress, and the measured mean and maximum grain size, is discussed. It is argued that both initial flaw size, e.g. a grain boundary and porosity must be considered in crack initiation stress prediction. The petrography of the starting material is described and the control of microstructure on fracture propagation modes is treated descriptively. The influence of porosity on mechanical parameters such as elastic modulus and ultimate stress is described. Finally, the combined influence of mean grain size, porosity and mosaic texture on crack initiation stress and ultimate strength is discussed.

2. Theoretical background

The mechanism of fracture initiation and propagation which lead to ultimate failure of rock under compression has been the subject for numerous publications. Early brittle fracture propagation studies were conducted by Brace and Bombalakis (1963) and by Hoek and Bieniawski (1965), who were able to observe the growth of cracks under compression in photoelastic material and glass. Brace and Bombalakis (1963) showed that in compression the most severely stressed crack is inclined at about 30 degrees to the axis of compression, and that it grows along a curved path which becomes parallel with the direction of compression. Hoek and Bieniawski showed that Griffith's theory for brittle fracture in a biaxial compressive stress field could only predict fracture initiation stress, and that the macroscopic failure of the rock occurs at higher stresses. Brace et al. (1966) explored the concept of rock dilation under confining pressures (up to 8 kbar) and showed that its onset can be identified with the point where the volumetric strain vs. axial stress curve deviates from the trend of elastic volume decrease, typically at about 50% of the peak stress for a wide variety of rocks. Bieniawski (1967) has postulated that stable fracture propagation starts at a lower stress level, about 35% of the peak stress, indicated by a change in linearity of the stress–strain curve. The onset of dilation point as defined by Brace et al. (1966) was interpreted by Bieniawski (1967) as an indication of the onset of unstable fracture propagation, typically at 80% of the peak stress.

The early studies have measured total volumetric strain from data of strain gages attached in parallel with the principal strain directions. These measurements include both the elastic component of volumetric strain and volumetric strain due to the formation of new crack volume. Martin and Chandler (1994) removed the elastic (linear) volumetric strain component from the total volumetric strain measured, and showed that the inelastic volume increase due to crack growth precedes Brace's onset of dilation point, and occurs at about 40% of the peak stress in Lac du Bonnet Granite. They have termed the point of initiation of new crack volume as crack initiation stress at which stable crack growth ensues.

There are several micromechanical models for fracture initiation in compression. These include: cylindrical pore, sliding crack, elastic mismatch, dislocation pile up, and Herztian crack models (Kemeny and Cook, 1991). In all models extensile cracking under compression seems to develop, as has been inferred by Zheng (1989) and Myer et al. (1992) using a petrographical study of thin sections containing injected Wood's metals. Although extensile cracking has been observed, the applicability of these models for the fracture of rock has not been validated experimentally. The most popular model for rocks of low porosity has been the 'sliding crack' model, perhaps because it has been observed in various compression tests on photoelastic materials (Brace and Bombalakis, 1963), glass (Hoek and Bieniawski, 1965), Columbia resin (Nemat-Nasser and Horii, 1982; Horii and Nemat-Nasser, 1985) and on PMMA (Ashby and Hallam, 1986). In all cases pre-cut flaws were introduced on the plate before loading. The stress intensity factor for crack initiation in an infinite plate using the sliding crack model has been approximated by Ashby and Hallam (1986). The mode I stress intensity factor, K_I, is found by seeking the plane θ on which the tensile stress is a maximum; and the most critical flaw is then identified by maximizing again, this time with respect to the flaw angle, y, giving the maximum K_I

as:

$$K_I = -\frac{\sigma_1\sqrt{\pi a}}{\sqrt{3}}\left[(1-\lambda)\sqrt{(1+\mu^2)} - (1+\lambda)\mu\right] \quad (1)$$

in the plane $\theta = 70.5°$ for the crack of angle $\psi = 0.5\tan^{-1}(1/\mu)$, where $\lambda = \sigma_1/\sigma_3$ (the ratio of principal stresses) and μ is the coefficient of friction. The condition for crack initiation is given by setting K_I equal to K_{Ic} (the fracture toughness of the material), giving the *initiation condition*:

$$\frac{\sigma_1\sqrt{\pi a}}{K_{Ic}} = \frac{-\sqrt{3}}{\left[(1-\lambda)\sqrt{1+\mu^2}\right] - (1+\lambda)\mu} \quad (2)$$

This solution is identical with Nemat-Nasser and Horii (1982) and similar in form to the solution of McClintock and Walsh (1962). The equation is strictly valid when the remote stress σ_{xx} is compressive because in tension the frictional component disappears. This fracture initiation criterion has been developed analytically assuming that the infinite plate is homogeneous and contains a single crack.

A good review of fracture initiation models is provided by Kemeny and Cook (1991) who also calculate the stress intensity factor associated with each mechanism. In the present study we test the applicability of the sliding crack model. The rock matrix is composed of rombohedral dolomite crystals where face to face and face to edge contacts are common, thus initial flaws are provided by faces of existing rombohedrons. The dolomite rombohedrons are oriented randomly in the rock matrix and it is assumed that there should be a crystal face oriented in the weakest direction at which the developed shear stress will exceed the shear strength of the rombohedron face. Stress concentration is proportional to the square root of the initial flaw size and is higher for longer crystal faces. Crack initiation is expected to start therefore from the edge of the largest crystal face which is also oriented most favourably. The crystal face which meets these conditions is assumed to be the critical flaw in the sample. Attainment of crack initiation stress should mark the initiation of sliding along that critical flaw.

The final stage of brittle rock deformation is macroscopic failure, defined here as the strain at which the maximum stress is achieved and referred to as ultimate strength. Beyond that point, post peak deformation is governed by specimen–machine interaction (Hudson et al., 1972) and is not analyzed here in detail. The point of peak stress represents the peak strength of the rock and therefore attempts have been made to predict it, empirically (Bieniawski, 1974; Coulomb, 1776; Hoek and Brown, 1980) and theoretically (Griffith, 1924). A good review of these criteria is given by Brady and Brown (1993).

3. Experimental procedures

3.1. The starting material

The rock samples used in the present study were taken from cores drilled through the Cenomanian Aminadav Formation in central Israel. The Aminadav Formation belongs to a sequence of Cretaceous platform dolomites, the composition of which is believed to be original (Sass and Katz, 1982). The manifestation of diagenetic processes is therefore limited to vugs which were formed by late dissolution, and recrystallization of secondary calcite, primarily in veins.

The formation consists of dolomite to slightly calcitic dolomite forming 1–2 m thick banks. Fresh fractured surfaces exhibit either dense, medium- to coarse-grained grey dolomite, or finely grained dolomite. The grain size exhibits a negative exponential distribution (Fig. 1), and the dominating texture is mosaic with three typical arrangements (Fig. 2). A detailed description of grain size distribution and mosaic texture is provided in Sections 4.1 and 4.2. The dolomites exhibit average bulk porosity of 7.98±4.4%. The porosity originates mainly from fabric-selective intercrystalline micropores, as well as vugs and microfractures which are not fabric-selective, according to the classification of Choquette and Lloyd (1970). The size of the intercrystalline micropores is in the order of several micrometres (Fig. 2). The vugs are typically circular with average diameter of 427±191 μm (Fig. 3a–c). The microfractures are elongated and are typically filled with calcite forming calcite veins; only in some cases do they remain open or reduced to vugs due to partial recrystallization (Fig. 3d). The length of the microfractures is in the order of one to several mm. Secondary recrystallization of calcite is found primarily in the veins (Fig. 3d), while the vugs retain their original open shape.

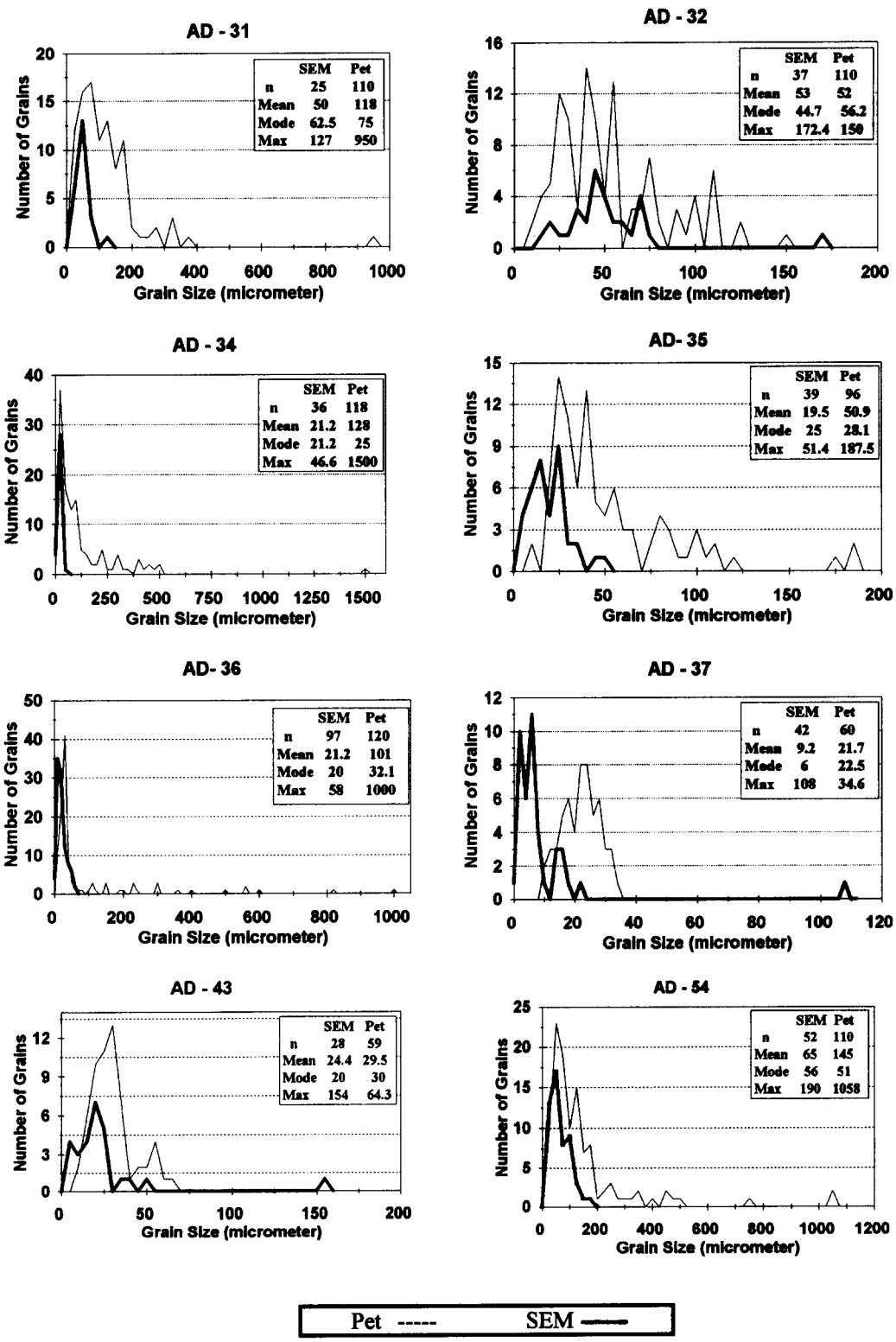

Fig. 1. Examples of eight grain size distributions using petrographic analysis (thin line) and scanning electron microscope (thick line).

Fig. 2. Typical mosaic textures in the studied dolomites: (a) *xenotopic* mosaic texture (SEM photo 9832); (b) *idiotopic* mosaic texture (SEM photo 4277); (c) *hypidiotopic* mosaic texture (SEM photo 7813).

3.2. Textural analysis

Petrographic analysis was performed using a petrographic microscope and a scanning electron microscope (SEM). The microstructure was studied before and after loading, in both methods. Grain size was measured using a calibrated reticule with crossline micrometer in a Zeiss petrographic microscope, and by direct measurements on scaled SEM micrographs. The size of vugs was measured on scaled optical micrographs. The results of these measurements enabled statistical analysis of grain size distribution in order to find mean grain size, modal grain size, and maximum grain size. The grain boundaries and packing were described and the proportions between the three prevailing mosaic textures were noted using both observation methods. Porosity was calculated using measured values of specific weight of solids (Gs), and measured dry density of the tested rock cylinders. Eight samples were ground for XRD analysis in order to detect the presence of minerals other than dolomite and calcite. The proportion between dolomite and calcite in the material were estimated using petrographic thin sections which were partially stained by Alizarin red, following procedures discussed by Tucker (1988). Table 1 shows the results of all the petrographic analyses, as well as the physical property data.

3.3. Rock testing

Samples of Aminadav dolomite were taken from cores of initially 80 mm in diameter. All sample preparation procedures comply in full with ISRM as well as ASTM standards, regarding end roughness, perpendicularity and L to D ratio. A nominal sample diameter of 54 mm was used in all tested cylinders. Testing was performed in the Rock Mechanics Laboratory of the Negev using a TerraTek triaxial testing system, model FX-S-33090. The stiff load frame operates using a closed-loop, servo-controlled hydraulic system of maximum axial force of 1.4 MN, stiffness of 5×10^9 N/m, and confining pressure capacity of 70 MPa. Control can be achieved using either load or displacement, thus constant strain rate or constant stress rate tests can be performed. All tests were run at a constant strain rate ranging between 1×10^{-5} and 5×10^{-6} s^{-1}. Piston

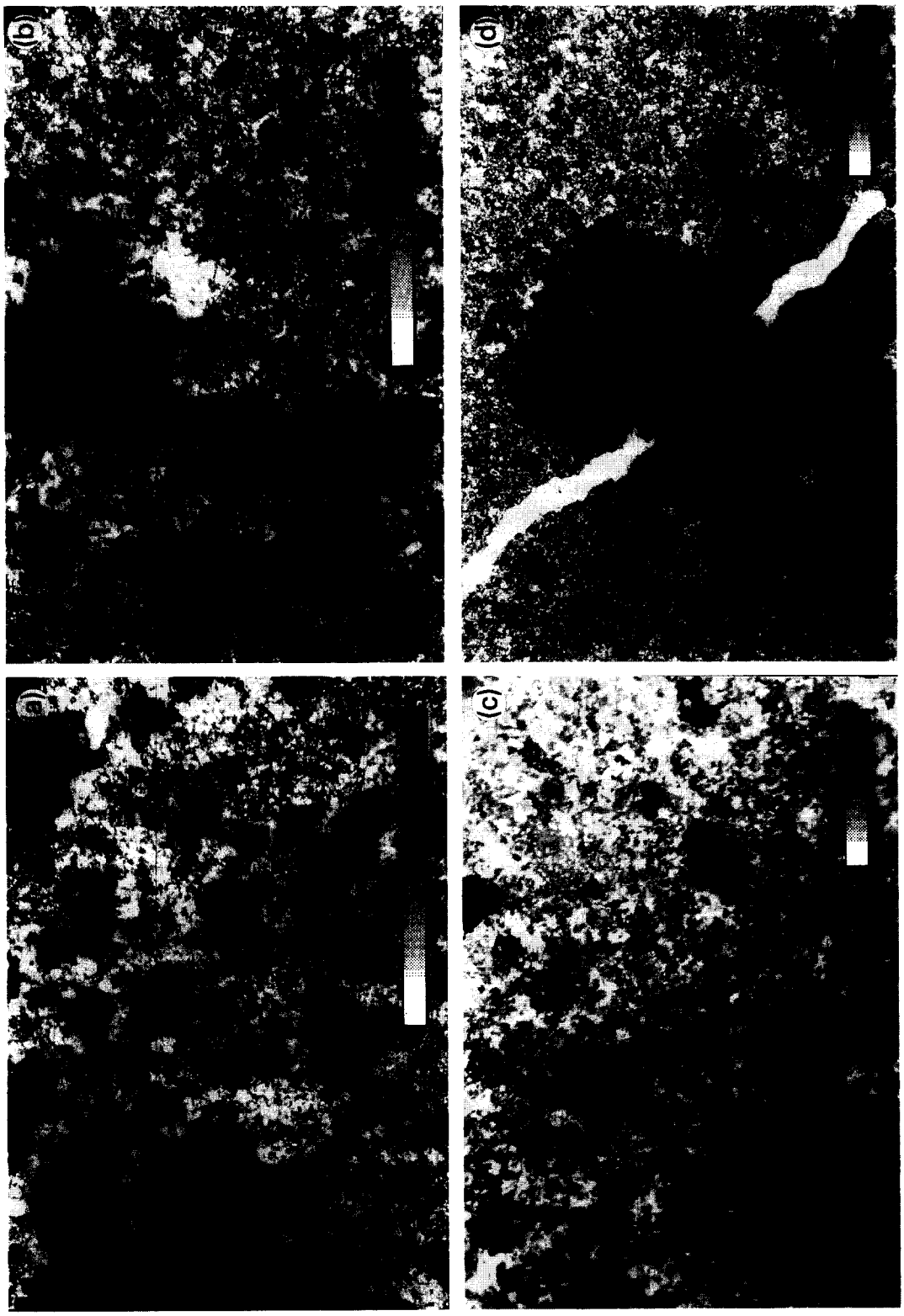

Fig. 3. Typical porosity types in the studied dolomites: (a) *vug* porosity in high-porosity rock (sample AD15, $n = 21\%$; (b) *vug* porosity in low-porosity rock (sample AD13, $n = 3.6\%$); (c) typical size distribution in a medium-porosity rock (sample AD81a, $n = 5.7\%$); original channel porosity reduced by calcite re-crystallization to *vug* type porosity in a medium-porosity rock (AD80, $n = 6.4\%$).

displacement was monitored using a high-sensitivity LVDT located outside the vessel near the piston. Load was measured by a sensitive load cell located in series with the sample stack having a maximum capacity of 1000 kN and linearity of 0.5% full scale. Sample axial and radial strains were recorded using four-arm axial and transverse strain cantilever sets, where arm deflection was calibrated to displacement (calibration was performed prior to testing). The axial cantilever set has a 10% strain range and the radial strain cantilevers have a strain range limit of 7%, with 1% linearity full scale for both sets. Several tests were performed without the internal axial and transverse strain cantilever systems, and axial displacement in these tests was inferred from the monitored stroke. These tests were only used for peak strength studies, as no information concerning true axial and transverse strain was acquired. Prior to testing, each sample was jacketed in a shrink tube to isolate the rock material from the pressure vessel oil. The complete stress–strain curves retrieved from testing all 32 samples were analyzed and the following mechanical parameters were defined: the elastic modulus (E), Poisson's ratio (ν), stress difference at crack initiation (σ_i), total volumetric strain at crack initiation (ϵ_i), stress difference at onset of unstable crack growth (σ_d), and stress difference at peak stress (σ_p). No reference has been made in this study to the post peak slope of the stress–strain curve.

3.4. Experimental repeatability

Axial and radial transducers were calibrated before and after the testing program using high accuracy dial gages which provided displacement readings for each cantilever arm independently. The repeatability of load and displacement readings in specimen scale was frequently verified between tests using two standard aluminum billets of different lengths, for which Young's modulus and Poisson's ratio were calculated in the elastic range, and compared with standard values reported by the manufacturer. In order to check actual repeatability of rock strength measurements two identical samples were tested in similar conditions: samples AD38A and AD38B under 20 MPa confining pressure. The physical properties of the two samples are listed in Table 1; the grain size data are common to both samples as they were studied from a thin section and a SEM specimen which represent both cylinders. Initial geometry and test conditions are listed in Table 2 together with strength results. The peak strength results differ by less than 2%, a difference which can be explained by different initial geometry. We are therefore certain that stress and strain results which are reported here, although noisy, reflect true material behaviour and not testing artifacts.

4. Results

4.1. Grain size distribution and critical crack length

Typical grain size distributions measured for eight different specimens are shown in Fig. 1. Generally the curves show a negative exponential trend, the frequency of which is relatively high for smaller grain sizes, and decreases exponentially with increasing grain sizes. Two observation techniques were employed, thin section analysis with the petrographic microscope and analysis of SEM photomicrographs. Eight representative examples are shown in Fig. 1. It can be seen that the global distribution is captured by thin section petrography, possibly because a larger area of the specimen was studied. The SEM observations give a more accurate picture of the grain population close to the mode of the global distribution. It can be seen that grain size distribution is quite wide. The size of grains within a single specimen may vary by two orders of magnitude in many cases. The frequency of the right tail of the distribution however is very low.

Using the available data it is necessary to determine which value should represent the most likely critical flaw size in terms of mechanistic analysis? Traditionally, workers have selected the mean grain size as the significant value in their interpretation of experimental results. Fracture mechanics considerations, however, predict highest stress concentrations at the tip of the longest flaw, which is oriented such that it mobilizes maximum shear stresses so that maximum tensile stresses develop at its tip. In the case of the studied dolomites, however, the longest flaws are the least expected. Furthermore, it can be shown that the probability that the longest grain is also critically oriented is extremely low. It is more likely that critically oriented cracks exist within the

Table 1
Physical properties and microstructure of tested samples

Sample	ρ (g/cm^3)	n (%)	Mosaic texture (%)			Fabric % crystals	Mineralogy % dolomite	Grain size (μm)	
			Xeno.	Idio.	Hypi.			mean (SEM)	max. (Pet)
AD2	2.75	2.0	80	–	20	100	80	49	260
AD5	2.62	5.8	50	10	40	80	70	35	450
AD6	2.63	6.4	5	15	80	95	90	11.8	45
AD11	–	–	30	20	50	98	95	27.6	130
AD13	2.68	3.6	40	10	50	100	92	25.2	450
AD15	2.19	20.9	25	40	35	100	80	33.5	173
AD18	2.58	7.9	15	45	40	85	85	17.4	70
AD19	2.59	7.5	35	–	65	100	90	13	97.8
AD31	2.59	7.47	30	40	30	90	85	–	–
AD31A	2.66	4.6	25	50	25	90	–	50	950
AD32	2.64	5.73	40	–	60	100	90	53	150
AD34	2.68	4.24	30	45	25	100	70	21.2	1500
AD35	2.6	7.1	5	30	65	75	60	19.5	188
AD36	2.61	6.74	30	–	70	95	85	21.2	1000
AD37	2.41	13.8	70	25	5	50	48	9.2	34.6
AD38A	2.61	6.6	–	15	85	100	85	21.5	740
AD38B	2.64	5.71	–	15	85	100	–	–	–
AD43	2.65	5.4	25	35	40	98	75	24.4	64.3
AD53	2.65	5.22	35	35	30	100	60	63.6	900
AD54	2.52	9.74	40	35	25	100	60	65	1058
AD60	2.38	14.7	–	75	25	80	65	17.5	113
AD63	2.71	3.12	40	15	45	95	79	30.6	450
AD66	2.68	4.16	15	–	85	100	95	16.6	300
AD80	2.62	6.4	10	20	70	95	79	26.9	375
AD81	2.61	6.8	10	80	10	70	25	27.5	250
AD81A	2.64	5.7	–	–	–	–	–	–	–
AD82	2.52	10	30	5	62.5	100	80	19.2	125
AD82A	2.43	13.2	–	–	–	–	–	–	–
AD83	2.37	15.4	70	–	30	100	80	27.3	375
AD83A	2.3	17.9	–	–	–	–	–	–	–
AD84	2.64	5.7	35	10	55	95	90	33.2	450

Legend: ρ = bulk density, n = bulk porosity, Xeno. = xenotopic, Idio. = idiotopic, Hypi. = hypidiotopic.

mode of the global grain size distribution. The mean of the petrographic distribution is affected by the right tail of the global distribution, whereas the SEM measurements are concentrated around the mode of the global distribution. Therefore the mean grain size value that is found using the SEM measurements may better describe the most likely length of the critical crack.

4.2. Microstructure patterns

Three dolomite mosaic textures are characteristic to the studied dolomites. The three types may co-exist within a single sample in varying proportions (see Table 1). The three types are defined below following the classification of Tucker and Wright (1990).

(1) Non-planar *xenotopic* mosaic texture, in which most dolomite crystals are anhedral rhombs characterized by irregular inter-crystalline boundaries, embedded in a fine-grained matrix of either dolomite or calcite. A SEM photograph of this texture is shown in Fig. 2a. This microstructure typically exhibits medium to low bulk porosity ($2\% < n < 10\%$).

(2) Planar *idiotopic* mosaic texture where most dolomite crystals are euhedral rhombs (Fig. 2b). This microstructure typically exhibits high bulk porosity ($10\% < n < 21\%$).

Table 2
Mechanical properties of tested dolomites

Sample	P_c (MPa)	L/D	ϵ_a (s^{-1})	E (GPa)	ν	σ_i (MPa)	σ_d (MPa)	σ_p (MPa)
AD2	0	2.03	5×10^{-6}	70	0.16	85	102	117
AD5	0	2.09	5×10^{-6}	56	0.37	83	85	98
AD6	0	1.99	1×10^{-6}	35	–	–	–	171
AD11	20	1.94	5×10^{-6}	67	0.28	200	235	254
AD13	10	2.05	5×10^{-6}	61	0.25	238	243	243
AD15	0	1.99	5×10^{-6}	29	0.26	39	57	67
AD18	7	2.04	5×10^{-6}	58	0.3	126	158	202
AD19	20	1.99	5×10^{-6}	56	0.31	–	–	241
AD31	10	2.01	5×10^{-6}	–	–	–	–	191
AD31A	15	1.9	1×10^{-6}	42	0.3	100	174	194
AD32	40	2.06	1×10^{-6}	–	–	–	–	286
AD34	25	2.11	1×10^{-6}	63.8	0.28	205	290	315
AD35	15	2.06	1×10^{-6}	–	–	–	–	228
AD36	30	2.05	1×10^{-6}	–	–	–	–	330
AD37	15	2.04	1×10^{-6}	28	0.35	130	138	142
AD38A	20	1.9	1×10^{-6}	–	–	–	–	275
AD38B	20	2.03	1×10^{-6}	–	–	–	–	280
AD43	0	2.04	1×10^{-6}	64	0.27	165	274	274
AD53	10	2.04	1×10^{-6}	–	–	–	–	303
AD54	25	1.93	1×10^{-6}	–	–	–	–	138
AD60	30	2.02	1×10^{-6}	–	–	–	–	246
AD63	35	2.1	1×10^{-6}	–	–	–	–	310
AD66	35	2.03	5×10^{-6}	–	–	–	–	343
AD80	0	2.1	1×10^{-6}	58.5	0.28	102	174	174
AD81	5	2.11	1×10^{-6}	59.2	0.18	90	110	154
AD81A	10	2.08	1×10^{-6}	57	0.27	135	230	255
AD82	10	2.08	1×10^{-6}	43	0.22	110	162	173
AD82A	15	2.04	1×10^{-6}	41	0.25	90	186	210
AD83	0	2.09	1×10^{-6}	18	0.25	43	43	62
AD83A	5	2.03	1×10^{-6}	19.6	0.24	45	52	70
AD84	10	2.08	1×10^{-6}	49.3	0.26	100	120	166

Legend: P_c = confining pressure, ϵ_a = axial strain rate, E = elastic modulus, ν = Poisson' ratio, σ_i = stress difference at crack initiation, σ_d = stress difference at unstable fracture, σ_p = peak stress difference.

(3) Planar subhedral *hypidiotopic* mosaic texture, in which most dolomite crystals are subhedral to anhedral with planar boundaries and common 'face to edge' crystal junctions (Fig. 2c). In this texture the bulk porosity is typically lower, between 2% and 6%.

4.3. Elasticity, dilatancy, and strength

In Table 2 all test results are shown including tests where in-vessel strain cantilever sets were not used. In these tests only peak strength data are listed. In one test (AD6) transverse strain data were not reliable, and in one test (AD19) the rock did not dilate at all during compression. In all other tests volumetric strain was monitored continuously and determination of crack initiation stress was performed by subtraction of the elastic volumetric strain from the total volumetric strain. The resulting curve is the 'crack volumetric strain' curve, the value of which is zero as long as deformation is purely elastic. The point of departure from zero crack volumetric strain marks the onset of crack initiation, the stress level of which is defined here as 'crack initiation stress'. Stress increase beyond crack initiation stress leads to rapid increase in crack volumetric strain and accordingly, to greater departure from the zero value. This method of detecting crack initiation stress is

reviewed in greater detail for example by Martin and Chandler (1994).

The elastic constants required for the calculation of the elastic volumetric strain were determined for each sample using linear regression performed on the linear segment of the stress–strain curve. The influence of confining pressure on the elastic constants was ignored here. The values of the elastic modulus were measured in the range between 18 GPa<70 GPa with an average modulus value of 49 ± 15 GPa. Poisson ratio values have a range of $0.16 < \nu < 0.35$ with an average value of 0.27 ± 0.05. Crack initiation stress is found at $\sigma_i/\sigma_p = 0.66 \pm 0.14$. These values are significantly higher than the values reported by Martin and Chandler (1994) for granite ($0.4\sigma_p$). Unstable cracking was found at $\sigma_d/\sigma_p = 0.87 \pm 0.1$, close to the value reported by Martin and Chandler (1994) for granite ($0.8\sigma_p$). Note that in some cases unstable crack growth and peak stress were attained coincidentally (Table 2). Unconfined compressive strength values have a range of 62 MPa<σ_c<274 MPa with an average value of $\sigma_c = 143 \pm 75$ MPa. The great scatter is due to the influence of microstructure. Two representative stress–strain curves of triaxial tests under equal confining pressure (10 MPa) for two samples of similar mean grain size but different bulk porosity are shown in Fig. 4. The influence of bulk porosity on strength is evident from inspection of these two curves, since all other parameters are equal.

In the next two sections the applicability of empirical and analytical criteria for failure, and the influence of microstructure on strength, are discussed.

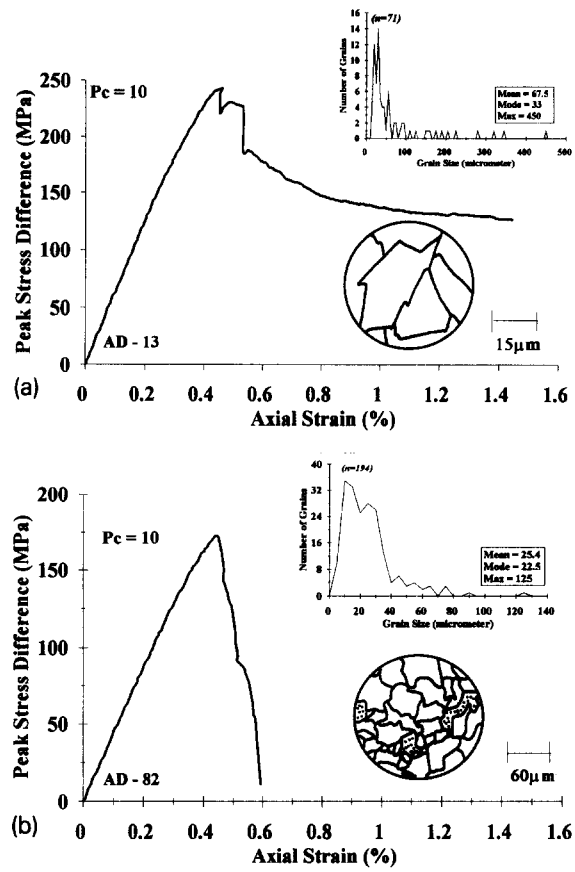

Fig. 4. Stress–strain curves for two samples of Aminadav dolomite, both of which are characterized by predominantly *hypidiotopic* mosaic texture: (a) sample AD13 of low porosity ($n = 3.6\%$) and high mean grain size ($d_m = 67.5\,\mu_m$); (b) sample AD82 of medium porosity ($n = 10\%$) and low mean grain size ($d_m = 25.4\,\mu_m$).

5. Applicability of failure criteria

5.1. Applicability of ultimate strength criteria

The most popular ultimate strength criterion for rock is the empirical Coulomb–Mohr failure criterion in which shear stress is given by two material properties: cohesion, and a poorly defined 'internal' friction angle. This failure criterion can be presented graphically using either shear and normal stresses, or principal stresses. More modern empirical failure criteria for rock, including Hoek and Brown (1980) and Bieniawski (1974) criteria, are scaled by the value of the unconfined compressive strength, which is assumed to be a material property, and require the use of one or two empirical constants, respectively. The analytical criterion of Griffith (1924) for failure in compression requires the unconfined compressive strength as the only necessary material property. Since the scatter of unconfined compressive strength values is found to be quite high in this study (Table 2) it is difficult to test the predictive capabilities of these criteria, since a single representative unconfined compressive strength value must be defined. In order to find 'representative' values, a regression for a Coulomb–Mohr criterion was performed using all test results and the following material properties were determined (Fig. 5): cohesion $c = 30$ MPa;

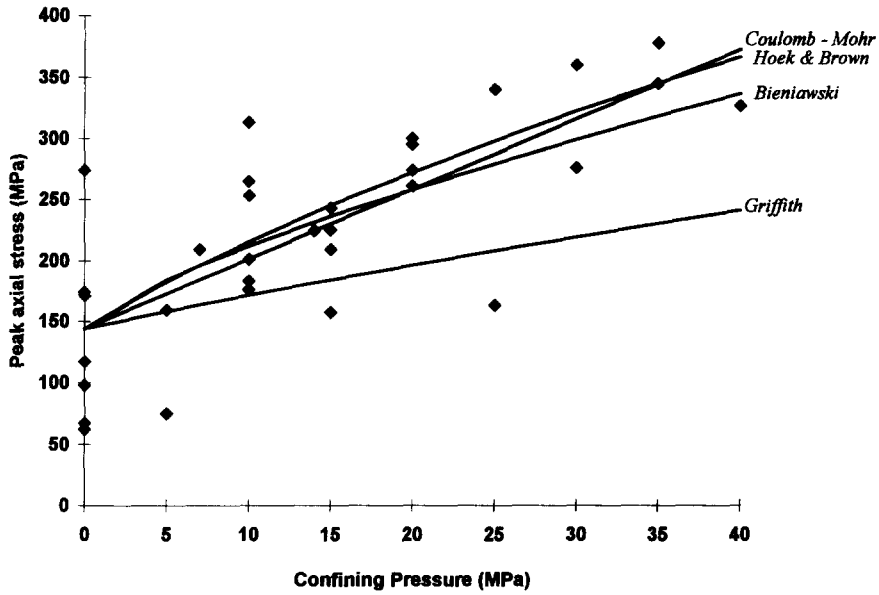

Fig. 5. Predictive capability of available failure criteria: classic failure criteria of Coulomb–Mohr (c = 30 MPa, ϕ = 44.6°, σ_c = 143 MPa), and Griffith (σ_c = 143 MPa), and empirical failure criteria of Bieniawski (A = 3.5, k = 0.75, σ_c = 143 MPa) and Hoek and Brown (m = 15, σ_c = 143 MPa).

peak internal friction angle (ϕ) = 44.6°; unconfined compressive strength (σ_c) = 143 MPa. It can be seen in Fig. 5 that while most tests plot near the best-fit line, several samples exhibit weaker behaviour, particularly when tested in unconfined compression. These lower strength results are explained below using microstructure considerations.

Using the best-fit σ_c value the predictive capabilities of the Griffith criterion as well as the empirical criteria can be evaluated. In Fig. 4 the Griffith criterion is plotted for σ_c = 143 MPa. It can be clearly seen that most samples exhibit higher ultimate strength values than predicted, primarily because of Griffith's assumption that once the propagation at the tip of critical cracks is initiated, sufficient energy exists for instantaneous fracture of the specimen. This has been shown to be incorrect, as crack initiation stress is detected at about 66% σ_p. Some samples, however, failed at stresses lower than Griffith's predicted failure stress, indicating that the average σ_c value that was used is not truly a representative material property.

Alternative failure criteria, based on a very large data base, are the empirical criteria of Bieniawski (1974) and Hoek and Brown (1980). The empirical criterion of Bieniawski (1974) requires two empirical constants: A and k and the unconfined compressive strength σ_c. A failure envelope calculated for A = 3.5 and k = 0.75 is shown in Fig. 4. The values A and k that were used are suggested by Bieniawski for the type of rocks which are tested here. The polynomial equation suggested by Bieniawski does capture the behaviour of most samples, except for the weaker members. The empirical equation of Hoek and Brown requires one constant: m and a material property σ_c. The value of m which gives a best fit is m = 15, similar to the value suggested by Brady and Brown (1993) for "arenaceous rock with strong crystals and poorly developed crystal cleavage (sandstone, quartzite)", and much higher than the value of 7.0 they suggested for dolomites. A failure envelope for the Hoek and Brown equation calculated for m = 15 and σ_c = 160 MPa is also shown in Fig. 4. Again, this empirical criterion captures the overall behaviour, with the exception of the weaker members.

In summary, empirical failure criteria seem to fit quite well the behaviour of the majority of the dolomites, with no consideration of microstructure. However, these criteria fail to predict the response of the weaker members in the same dolomite formation. The analytical model of Griffith is not applicable, it

underestimates the strength of the majority of the samples, yet it over estimates the strength of the weaker members.

5.2. Applicability of fracture initiation criteria

An analytical fracture initiation criterion for rock under compression was proposed by Ashby and Hallam (1986) (Eq. 2 above) for a critically oriented crack using fracture mechanics and assuming the sliding crack model and a mode I stress intensity factor (K_{Ic}). If we assume that a grain boundary functions as a potential Griffith flaw, then a correlation would be expected between the calculated flaw size ($2a$) at crack initiation stress (σ_i) by the analytical model, and the critical grain size in a given sample. We have argued above that the most likely grain size is represented by the mean of the grain size distribution measured using SEM, whereas stress concentrations are highest at the tip of the largest flaw in a given sample, provided it is appropriately oriented. It is difficult, however, to predict whether crack propagation will ensue from the tip of the most likely or the longest crack.

A comparison between model prediction of critical flaw length, and actual measurement of most likely and longest crack, is performed here for all tests for which a crack initiation stress was inferred (19 tests, Table 2). A stress intensity factor of 1.8 MPa $m^{0.5}$ was assumed using experimental data for dolomite published by Atkinson and Meredith (1987), and a friction coefficient of 0.98 was used, assuming the mean friction angle value found in this study (Fig. 5). The results of the comparison between the calculated flaw size at crack initiation stress and the observed mean and maximum grain size are shown in Fig. 6a and b, respectively. Clearly there is no correlation between calculated and measured values. The measured mean grain size values (using SEM) range between 10 and 50 μm, and the measured maximum grain size values (using petrographic microscope) range between 35 and 1,500 μm. The range of required flaw size for initiation, under the measured crack initiation stress and the assumed K_{Ic} value, is between 780 and 95,000 μm, assuming the Ashby and Hallam model. Although the analytical model attempts to give a rough estimate under simplifying assumptions, the discrepancies are too severe, and amount to a difference between predicted and measured values of up to three orders of magnitude.

According to the analytical model prediction fracture should ensue at much higher stresses than observed. That would have been the case had fracture been controlled by stress concentrations at the tip of critically oriented grain boundaries only. In fact, the rock is much weaker, and fracture propagation and growth ensues at much lower stress levels than predicted. It is suggested therefore that other processes control fracture initiation and propagation, the mechanisms of which are influenced to a large extent by micro-crystalline arrangement. The influence of microstructure on mechanical behaviour is examined in the next section.

6. The influence of microstructure on mechanical strength

6.1. The influence of grain size

Several investigators have shown that for a variety of sedimentary rocks a correlation between mean grain size and ultimate strength exists, either a linear correlation with the inverse square root of the mean grain size (Olsson, 1974; Fredrich et al., 1990), or negative exponential with the mean value (e.g. Hugman and Friedman, 1979; Wong et al., 1995).

In Fig. 7 maximum (petrographic microscope) and mean (SEM) grain size values are plotted against stress difference at crack initiation (σ_i) and at ultimate strength (σ_p). It can be seen that peak and crack initiation stresses are independent of the maximum grain size in the specimen (Fig. 7a). This result supports our assumption that the likelihood that low frequency sizes are also properly oriented is quite low.

A weak dependence of crack initiation and peak stresses on mean grain size value is indicated by the results of this study (Fig. 7b). The existing, albeit weak, correlation supports our assumption that mean grain size values captured by SEM observations are more likely to function as critical cracks in the samples. This result is in general agreement with the earlier studies mentioned above. However, the weak correlation suggests that additional geometric factors must be considered. The most obvious in the case

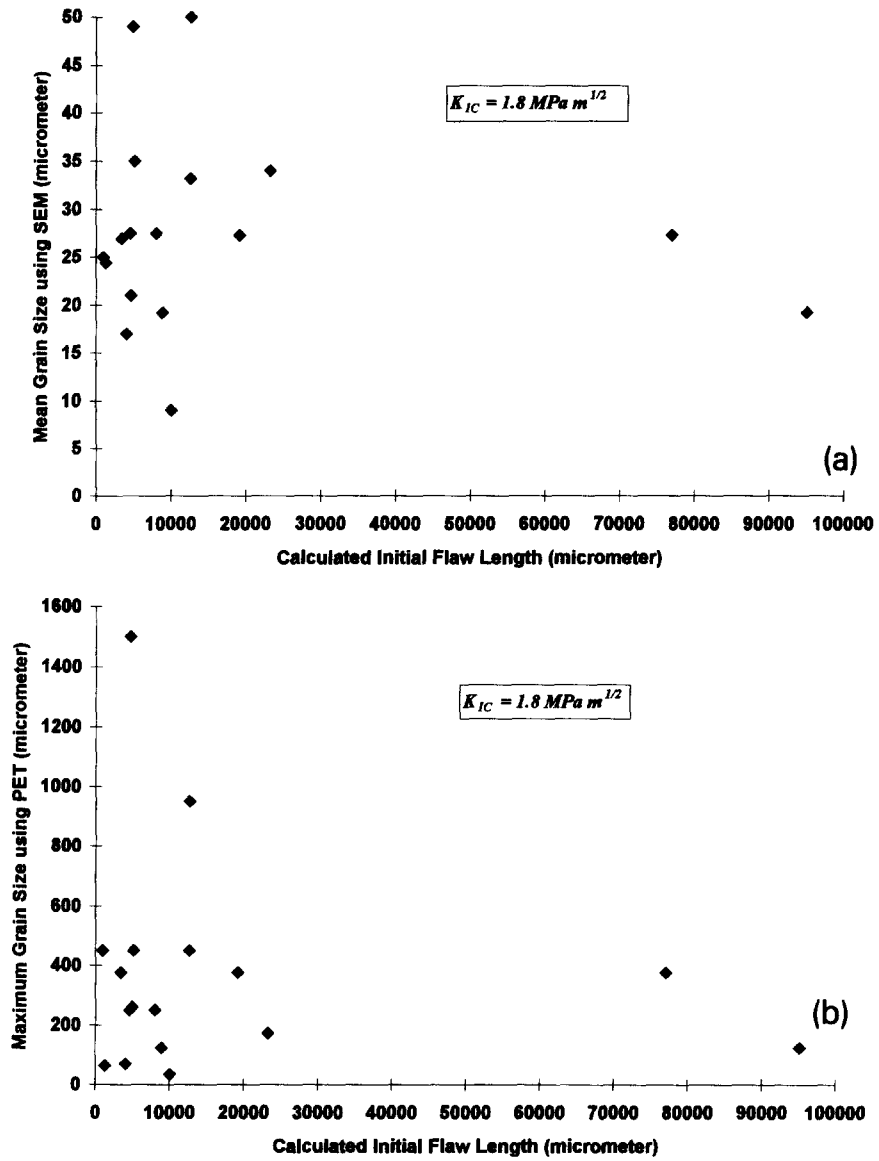

Fig. 6. Comparison between critical flaw size at crack initiation stress using the initiation criterion of Ashby and Hallam (1986), and the observed grain size in this study: (a) comparison with mean grain size (SEM observations); (b) comparison with maximum grain size (petrographic thin sections).

of the studied dolomites are porosity and mosaic texture, the influence of which are explored below.

It should be noted that better correlation exists between mean grain size and crack initiation stress ($R^2 = 0.09$, power law) than between mean grain size and ultimate stress ($R^2 = 0.02$, power law). This result is to be expected. The theoretical basis for the correlation between strength and grain size is Griffith's fracture criteria which can be generalized in the following form (Atkinson, 1987):

$$K = Y\sigma\sqrt{\pi c} \tag{3}$$

where K is a general stress intensity factor, σ is the remote applied stress, Y is a numerical modification factor which accounts for crack geometry, loading conditions and edge effects, and c is half crack

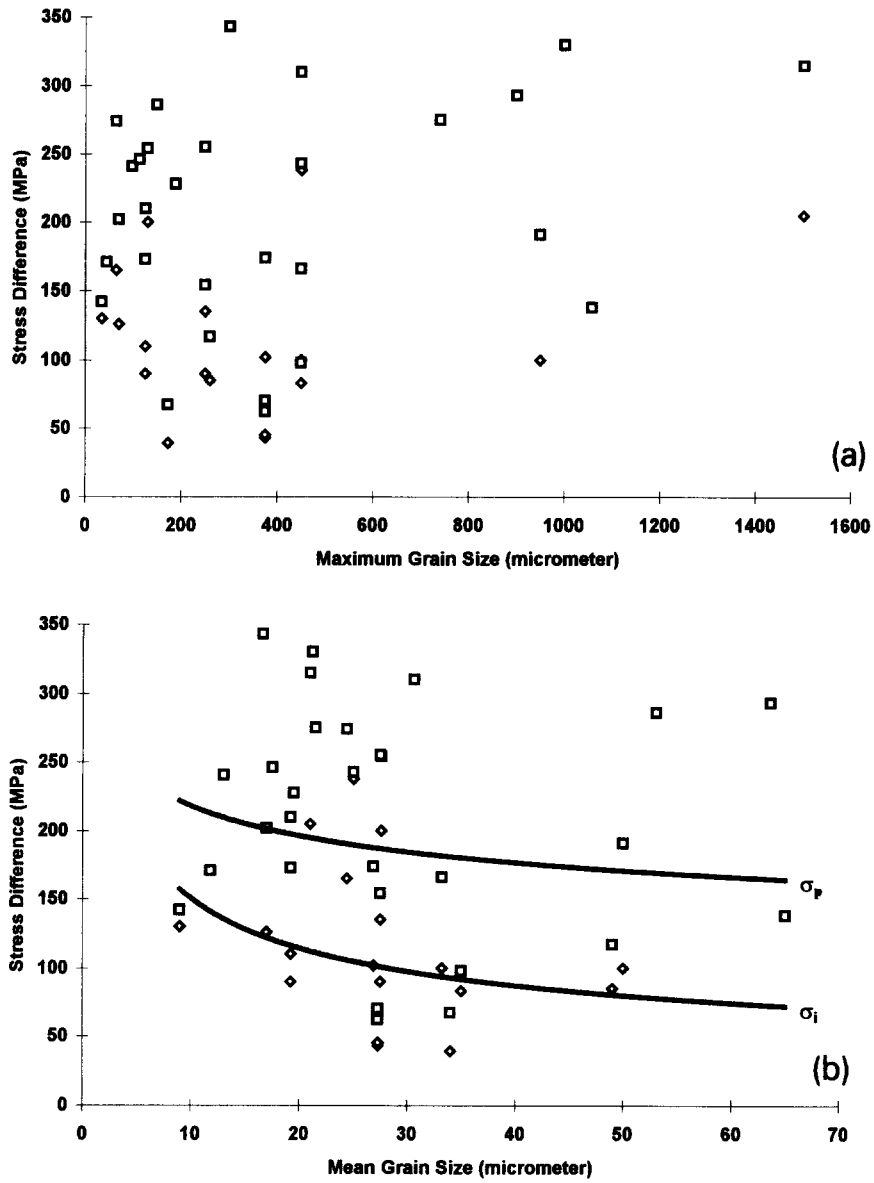

Fig. 7. Correlation between stress difference and grain size: (a) maximum grain size measured using petrographic microscope, (b) mean grain size measured using SEM. Legend: ◇ = stress difference at crack initiation (σ_i); □ = peak stress difference (σ_p).

length. In this criterion stress intensity is directly proportional to the square root of the initial flaw size, and hence the expected correlation between strength and grain size. This criterion, however, is formulated for initiation, a process that has been shown here to take place at about 66% of the maximum stress level. The value of the remote stress at failure, the ultimate stress level, must be influenced by fracture growth and interaction processes which are ignored in Eq. 3.

6.2. *The influence of porosity*

The influence of bulk porosity on strength in sandstone was discussed by Dunn et al. (1973) and Scott and Nielsen (1991), and the prediction of porosity

using seismic velocities was discussed by Vernik and Nur (1992), among others. Vernik et al. (1993) have developed empirical criteria for shear strength of siliciclastic rocks using results of unconfined and triaxial compression tests with porosity data from sedimentary basin rock lithologies. The inverse relationship between bulk porosity and ultimate strength has been noted by all studies mentioned above, which were focused on reservoir source rocks: siliciclastics and pure sandstones.

In this research the influence of porosity on crystalline dolomites with varying microstructures is studied. The three microstructures (Fig. 2) typically appear together in a given sample at varying proportions (Table 1). The fabric-dependent *intergranular* porosity can be used as a scaling parameter for this proportion. In idiotopic mosaic texture, where individual grains are embedded in a matrix, or fill voids (Fig. 2b), the intergranular porosity is expected to be at the high extreme. In hypidiotopic mosaic, where compromise boundaries between adjacent grains are common (Fig. 2c), the intergranular porosity is expected to be at the lower end. Therefore, as intergranular porosity values decrease, the specimen is expected to exhibit greater proportions of hypidiotopic texture. It could be argued (see Section 7) that fracture propagation requires higher stresses with increasing proportion of hypidiotopic texture, due to common edge to face junctions. If this assumption is correct, than strength and intergranular porosity should be inversely related. The micropores which are not fabric-dependent, the vugs (Fig. 3), may function as stress concentrators, and ultimate stress at fracture should be inversely related to their diameter (see for example the analytical solution of Sammis and Ashby, 1986).

In this research the *bulk* porosity is measured and no quantitative distinction is made here between fabric-dependent and fabric-independent porosity. Such a distinction however is not essential because both types of porosity, the sum of which is represented by the value of the bulk porosity, have similar effects on rock strength.

In Fig. 8a the relationship between stress difference and porosity is shown at crack initiation and ultimate stress. The expected inverse relationship between strength and porosity is confirmed by the results, and as in the case of grain size, the data set for crack initiation stress yields a higher correlation coefficient for exponential fit ($R^2_{\sigma_i} = 0.53$; $R^2_{\sigma_p} = 0.41$).

The bulk porosity has a pronounced effect on the elastic response of the rock. In Fig. 8b porosity values are plotted against the elastic modulus for all tests where axial displacement was monitored directly on the sample (19 tests). The inverse relationship between Young's modulus and porosity is quite clear ($R^2_{\text{exp. fit}} = 0.7$). This relationship probably reflects the proportional increase in compressible cement with respect to incompressible crystals, as porosity is increased.

Finally, bulk porosity can be used to re-examine the ultimate strength results which were obtained in this study and discussed above. In Fig. 9 peak axial stress is plotted against confining pressure in a typical σ_1, σ_3 space. The data are clustered into four groups of similar porosity values and two linear regression lines are plotted, for medium porosity ($6.6\% < n < 9.7\%$) and high porosity ($9.7\% < n < 21\%$). The linear regression for these two groups yields reasonable correlation coefficients, $R^2_{\text{low porosity}} = 0.95$ and $R^2_{\text{high porosity}} = 0.74$, respectively. The relatively high correlation coefficients calculated for correlation with bulk porosity, in comparison to correlation with mean grain size, indicate that failure of polycrystalline dolomites is more influenced by variations in bulk porosity than in mean grain size.

7. Discussion

In the previous sections it has been shown that grain size and porosity influence the mechanical behaviour of a polycrystalline aggregate such as dolomite. It has been shown that ultimate strength in such rocks is not a simple function of classical material properties such as cohesion and internal friction angle, as suggested by the linear Mohr–Coulomb failure criterion (Fig. 4). Neither can ultimate strength be predicted using a representative unconfined compressive strength value (σ_c) as suggested by the Griffith criterion and the investigated empirical criteria (Fig. 4), because σ_c is not a true material property; within the same dolomite formation σ_c values were shown to vary by a factor of 2.8 (compare AD5 and AD43 in Table 2 with similar

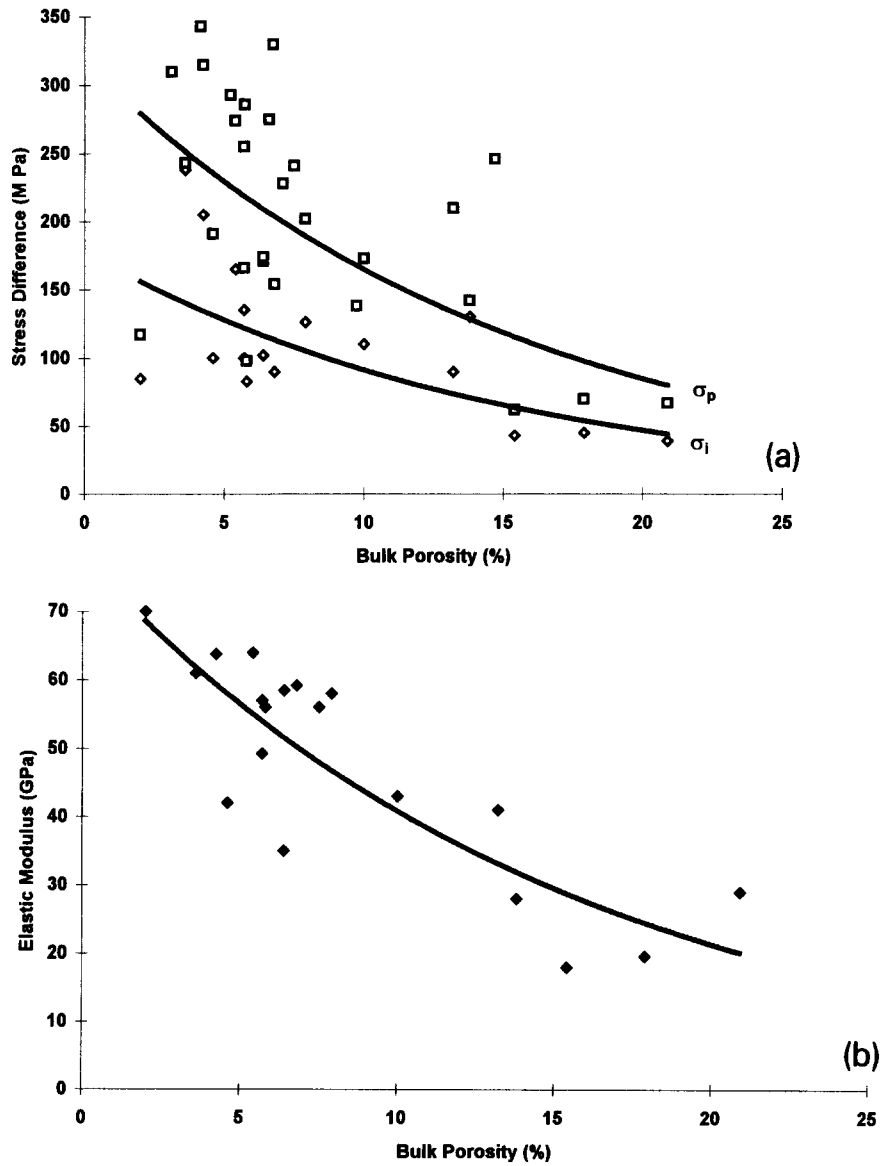

Fig. 8. (a) Influence of porosity on stress difference at crack initiation ($R^2_{\text{exponential fit}} = 0.53$) and on peak stress difference ($R^2_{\text{exponential fit}} = 0.41$). Legend: ◇ = stress difference at crack initiation (σ_i); □ = peak stress difference (σ_p); (b) influence of porosity on the elastic modulus ($R^2_{\text{exponential fit}} = 0.7$).

percent dolomite and porosity in both samples). The two microstructure components that were studied, grain size distribution and porosity, are completely overlooked in all failure criteria, hence the poor predictive capability.

It has been common to assume that grain size is the dominant factor controlling strength, to a large extent due to predictions of fracture mechanics models. This study clearly shows that grain size, although important, is not the controlling factor. Furthermore, comparison between predicted critical flaw size using available fracture initiation criteria and actual observations show that the predicted initial flaw size is larger than the observed one by two to three orders of magnitude, namely the studied rocks are much *weaker* than predicted when measured grain

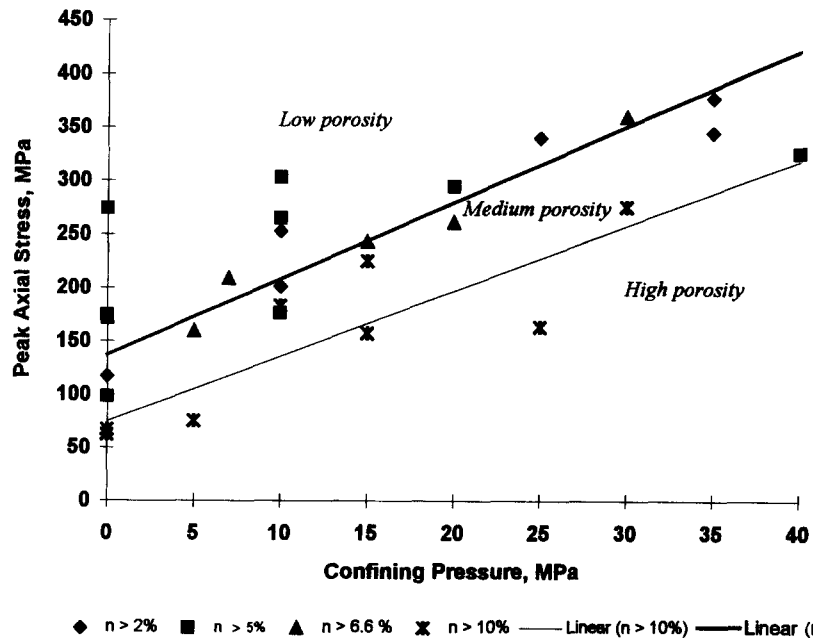

Fig. 9. Coulomb–Mohr failure envelopes for dolomites of varying porosity: low porosity ($n < 6.6\%$), medium porosity ($6.6\% < n < 10\%$), high porosity ($n > 10\%$). Linear regression coefficients: $R^2_{(n<6.6\%)} = 0.95$; $R^2_{(n>10\%)} = 0.74$.

size is used as the initial flaw size. This discrepancy indicates the importance of other geometric factors which comprise rock fabric. It has been shown that porosity has a greater effect on the elastic response, fracture initiation, and ultimate stresses, than the value of the mean grain size.

The discrepancies between conventional fracture initiation and failure criteria and actual observations can be explained if we consider two alternative fracture propagation mechanisms, which depend upon mosaic texture, and are qualitatively discussed below:

(1) *Inter-crystalline* fracture propagation, in which fractures propagate between crystal boundaries, is expected to be dominant in *idiotopic* and *xenotopic* mosaic textures (Fig. 2a and b). In this mechanism a grain boundary which is properly aligned with respect to the major principal stress direction is the initial flaw, as in the case of the sliding crack model. When the developed shear stresses across the inclined plane are greater than its shear strength, the fracture propagates between grain boundaries, a process which requires relatively low mechanical energy. An example of such a fracture is shown in Fig. 10a, which was photographed from the vicinity of the failure zone in a sample which experienced failure under a confining pressure of 10 MPa (sample AD13).

(2) *Intra-crystalline* propagation, in which crack propagation is enabled only by splitting fracture through neighbouring crystals, is expected to be dominant in *hypidiotopic* textures (Fig. 2c). In this mechanism the initial flaw is an inclined plane of a crystal boundary which is embedded in an adjoining crystal mass. When the developed shear stresses across this plane are greater than its shear strength, propagation is induced. However, in order for the crack to propagate through the surrounding mass, the stress concentration at its tip must overcome the fracture toughness of the intact dolomite crystal, a process which requires relatively high mechanical energy. An example of an intracrystalline fracture is shown in Fig. 10b, a SEM photograph from the vicinity of the failure zone of sample AD53 which was tested under a confining pressure of 10 MPa.

We have seen that at least three microstructure parameters control the failure of dolomites. The mean grain size length and the mean pore diameter control the magnitude of stress concentrations at the tip of the leading cracks. The mosaic texture controls

Fig. 10. Two fracture propagation mechanisms in crystalline dolomites: (a) *inter-crystalline* fracture propagation, typically observed in *xenotopic* mosaic texture; (b) *intra-crystalline* fracture propagation mechanism, typically detected in *hypidiotopic* mosaic texture.

the required fracture initiation stress and the fracture propagation mechanism. Hatzor and Palchik (1997) developed an empirical model for fracture initiation stress as composite function of both porosity and mean grain size, using an assumption that porosity scales mosaic texture. They have shown empirically that fracture initiation stress is inversely related to both mean grain size and porosity. They have found that the influence of grain size on crack initiation stress is more pronounced in low-porosity than in high-porosity rocks, and that the influence of porosity on crack initiation stress is more pronounced in rocks of low grain size. Furthermore, they have shown analytically that the initial flaw length is also proportional to porosity and mean grain size, and that only in the extreme case of low porosity–low grain size does the initial flaw length coincides with the mean grain size of the rock.

While empirical models for fracture initiation stress as a function of both porosity and grain size can be developed, predicting ultimate strength is much more difficult. The difficulty stems from the fact that ultimate stress is attained after complex fracture propagation processes, which highly depend upon mosaic texture, take place. Yet as has been shown (see Table 1), the mosaic texture is not constant in a given rock and could vary from place to place in a given specimen. However, it has been shown here that using bulk porosity values (Fig. 9) the value of ultimate stress can be estimated reasonably well.

8. Summary and conclusions

The influence of microstructure on the mechanical behaviour of dolomites has been studied, particularly the effect of grain size and porosity on crack initiation stress and ultimate strength. The same type of grain size distribution was calculated from petrographic analysis and SEM observations, and is typically of the form of a negative exponential. It is argued that the initial length of the critical flaw in the sample is most likely represented by the mean rather than the maximum of the distribution, and therefore mean grain size is used to scale initial flaw length. Three mosaic textures are identified, xenotopic, idiotopic, and hypidiotopic, all of which may co-exist in a single specimen at varying proportions.

The predictive capability of empirical failure criteria is shown to be quite weak, and it is argued that this is because fabric constraints are ignored. Similarly the modified Griffith criterion for failure is not applicable because it uses unconfined compressive strength as a constant material property, which is shown here to be highly dependent upon fabric.

Analytical model predictions for crack initiation stress are used inversely to find the critical flaw length in the sample, when crack initiation stress is used as the remote stress input. It is found that the predicted critical flaw length is larger by one to two orders of magnitude than the observed, namely, the rocks fail at lower remote stresses than required by

the available initial flaw length (mean grain size). It is argued that the discrepancy is largely due to the negligence of different boundary conditions which are active in the case of the idealized sliding crack model, when different mosaic textures are present.

The actual influence of mean grain size and porosity on crack initiation stress and ultimate strength has been studied. It was shown that both crack initiation and ultimate stresses are relatively insensitive to mean grain size but are very sensitive to the value of porosity. This is also demonstrated by the construction of Coulomb–Mohr failure envelopes for clusters of data of equal porosity, which yield very reasonable correlation coefficients (up to 0.95).

It may be concluded that the role of mean grain size and porosity as stress concentrators is of supreme importance. However, once sufficiently high stresses are developed and fracture is initiated, the nature of grain arrangement imposes a constraint on the micromechanics of fracture growth. Therefore, ultimate stress level is controlled by the nature of mosaic texture, which to some extent is scaled by porosity.

Acknowledgements

This research was supported by a grant from the Earth Science Administration, the Ministry of Energy and Infrastructure, State of Israel, through contracts Nos. 93-17-022 and 94-17-041. An early version of the manuscript was read by Yves Bernabe and his comments were very useful. We thank E.H. Rutter and an anonymous reviewer for their critical review of the paper. Their remarks and suggestions greatly improved the quality of the manuscript.

References

Ashby, M.F., Hallam, S.D., 1986. The failure of brittle solids containing small crack under compressive stress states. Acta Metall. 34, 497–510.

Atkinson, B.K., 1987. Introduction to fracture mechanics and its geophysical applications. In: Atkinson, B.K. (Ed.), Fracture Mechanics of Rock. Academic Press, London, Chap. 1.

Atkinson, B.K., Meredith, P.G., 1987. Experimental fracture mechanics data for rocks and minerals. In: Atkinson, B.K. (Ed.), Fracture Mechanics of Rock. Academic Press, London, Chap. 11.

Bieniawski, Z.T., 1967. Mechanism of brittle fracture of rock, Part II. Experimental studies. Int. J. Rock Mech. Min. Sci. Geomech. Abstr. 4, 407–423.

Bieniawski, Z.T., 1974. Estimating the strength of rock materials. J. S. Afr. Inst. Min. Metall. 74, 312–320.

Brace, W.F., Bombalakis, E.G., 1963. A note on brittle crack growth in compression. J. Geophys. Res. 68, 3709–3713.

Brace, W.F., Paulding, B.W., Scholz, C., 1966. Dilatancy in fracture of crystalline rocks. J. Geophys. Res. 71, 3939–3953.

Brady, B.H.G., Brown, E.T., 1993. Rock Mechanics for Underground Mining, 2nd ed. Chapman and Hall, London, 571 pp.

Choquette, P.W., Lloyd, C.P., 1970. Geologic nomenclature and classification of porosity in sedimentary carbonates. Am. Assoc. Pet. Geol. Bull. 54, 207–250.

Coulomb, C.A., 1776. Essai sur une application des règles de maximis et minimis à quelque problèmes de statique, relatifs à l'architecture. Mem. Math. Phys., Acad. R. Sci. 7: 343–382.

Dunn, D.E., La Fountain, L.J., Jachson, R.E., 1973. Porosity dependence and mechanisms of brittle fracture in sandstones. J. Geophys. Res. 78, 2403–2417.

Fredrich, J.T., Evans, B., Wong, T.F., 1990. Effects of grain size on brittle and semibrittle strength: implications for micromechanical modelling of failure in compression. J. Geophys. Res. 95, 10907–10920.

Griffith, A.A., 1921. The phenomena of rupture and flow in solids. Philos. Trans. R. Soc. London, A 221, 163–197.

Griffith, A.A., 1924. Theory of rupture. Proc. 1st Congr. Applied Mechanics, Delft, pp. 55–63.

Handin, J., Fairbairn, W.H., 1955. Experimental deformation of Hasmark dolomite. Geol. Soc. Am. Bull. 66, 1257–1274.

Handin, J., Hager, R.V., 1957. Experimental deformation of sedimentary rocks under confining pressure: tests at room temperature on dry samples. Am. Assoc. Pet. Geol. Bull. 41, 1–50.

Hatzor, Y.H., Palchik, V., 1997. The influence of grain size and porosity on crack initiation stress and critical flaw length in dolomites. Int. J. Rock Mech. Min. Sci. Geomech. Abstr., in press.

Hoek, E., Bieniawski, Z.T., 1965. Brittle fracture propagation in rock under compression. Int. J. Fracture Mech. 1, 139–155.

Hoek, E., Brown, E.T., 1980. Underground Excavation in Rock. Inst. Min. Metall., London.

Horii, H., Nemat-Nasser, S., 1985. Compression induced microcrack growth in brittle solids: axial splitting and shear failure. J. Geophys. Res. 90, 3105–3125.

Hudson, J.A., Crouch, S.L., Fairhurst, C., 1972. Soft, stiff and servo-controlled testing machines: a review with reference to rock failure. Eng. Geol. 6, 155–189.

Hugman, R.H.H., Friedman, M., 1979. Effects of texture and composition on mechanical behavior of experimentally deformed carbonate rocks. Am. Assoc. Pet. Geol. Bull. 63, 1478–1489.

Kemeny, J.M., Cook, N.G.W., 1991. Micromechanics of deformation in rocks. In: Shah, S.P. (Ed.), Toughening Mechanisms in Quasi-Brittle Materials. Kluwer Academic Publishers, Dordrecht, pp. 155–188.

Martin, C.D., Chandler, N.A., 1994. The progressive fracture

of Lac du Bonnet Granite. Int. J. Rock Mech. Min. Sci. Geomech. Abstr. 31, 643–659.

McClintock, F.A., Walsh, J.B., 1962. Friction of Griffith cracks in rocks under pressure. In: Proceedings of the U.S. National Congress on Applied Mechanics, 4th Vol. II. American Society of Mechanical Engineers, New York, pp. 1015–1021.

Myer, L.R., Kemeny, J., Cook, N.G.W., Suarez, R., Zheng, Z., 1992. Extensile cracking in porous rock under differential compressive stress. Applied Mech. Rev. 45 (8), 263–280.

Nemat-Nasser, S., Horii, H., 1982. Compression-induced nonplanar crack extension with application to splitting, exfoliation and rockburst. J. Geophys. Res. 87, 6805–6821.

Olsson, W.A., 1974. Grain size dependence of yield stress in marble. J. Geophys. Res. 79, 4859–4862.

Petch, N.J., 1953. The cleavage strength of polycrystals. J. Iron Steel Inst. 174, 25–28.

Sammis, C.G., Ashby, M.F., 1986. The failure of brittle porous solids under compressive stress state. Acta Metall. 34, 511–526.

Sass, E., Katz, A., 1982. The origin of platform dolomites: new evidence. Am. J. Sci. 282, 1184–1213.

Scott, T.E., Nielsen, K.C., 1991. The effects of porosity on the brittle–ductile transition in sandstones. J. Geophys. Res. 96, 405–414.

Tucker, M.E., 1988. Techniques in Sedimentology. Blackwell Scientific Publications, Oxford, 394 pp.

Tucker, M.E., Wright, V.P., 1990. Carbonate Sedimentology. Blackwell Scientific Publications, Oxford, 482 pp.

Vernik, L., Nur, A., 1992. Petrophysical classification of siliciclastics for lithology and porosity prediction from seismic velocity. Am. Assoc. Pet. Geol. Bull. 9, 1295–1309.

Vernik, L., Buno, M., Bovberg, C., 1993. Empirical relations between compressive strength and porosity of siliciclastic rocks. Int. J. Rock Mech. Sci. Geomech. Abstr. 30 (7), 677–680.

Weiss, L.E., Turner, F.J., 1972. Some observations of translation gliding and kinking in experimentally deformed calcite and dolomite. In: Heard, H.C., Borg, I.Y., Carter, N.L., Raleigh, C.B. (Eds.), Flow and Fracture of Rocks. Am. Geophys. Union, Geophys. Monogr. 16, 95–108.

Wong, H.C., Chau, K.T., Wang, P. 1995. Microcracking in coarse and fine grain marbles. In: Daemmen, J.J.K., Schultz, R.A (Eds.), Rock Mechanics. Balkema, Rotterdam, pp. 477–482.

Zheng, Z., 1989. Compressive Stress-Induced Microcracks in Rocks and Applications to Seismic Anisotropy and Borehole Stability. Ph.D. Thesis, University of California, Berkeley.